Pergamon

Int. J. Heat Mass Transfer. Vol. 39, No. 13, pp. 2723–2733, 1996

0017-9310/96 $15.00+0.00

0017-9310(95)00360-6

Modeling the local and average heat transfer coefficient for an isothermal vertical flat plate with assisting and opposing combined forced and natural convection

C. J. KOBUS and G. L. WEDEKIND†

School of Engineering and Computer Science, Oakland University, Rochester, MI 48309, U.S.A.

(*Received* 15 *May* 1995 *and in final form* 19 *September* 1995)

Abstract—A theoretical model is formulated, utilizing an integral technique, to describe the thermal boundary layer development. Special case closed-form solutions are obtained for $0.72 \leqslant Pr \leqslant 10$ to predict the local and average heat transfer coefficient for combined forced and natural convection from an isothermal vertical flat plate, for both assisting and opposing flows. No opposing flow closed-form solutions are known to exist in the current literature. Assisting and opposing flow experiments were performed to measure the average heat transfer coefficient with air for two flat plate heat transfer models of different lengths. The predictive capability of the present theoretical model was compared to this experimental data with excellent agreement. Excellent agreement is also found to exist with the experimental data and numerical solutions of other researchers. Copyright © 1996 Elsevier Science Ltd.

INTRODUCTION

The mode of convective heat transfer which is neither dominated by pure forced nor pure natural convection, but is rather a combination of the two, is referred to as combined forced and natural convection. In such instances, the relative direction between the buoyancy force and the externally forced flow is important. In the case where the fluid is externally forced to flow in the same direction as the buoyancy force, the mode of heat transfer is termed *assisting* combined forced and natural convection. In the case where the fluid is externally forced to flow in the opposite direction to the buoyancy force, the mode of heat transfer is termed *opposing* combined forced and natural convection.

A survey of the literature indicates that there has been less research in the case of combined forced and natural convection than for either pure forced or pure natural convection. A good summary of the existing research is given by Churchill [1] and more recently by Gebhart *et al.* [2]. A number of theoretical papers [3–14] and some limited experimental data [8, 15–18] exist in the literature. However, a general closed-form solution to the combined problem has not, to the best knowledge of the authors, been presented. The intent of this paper is to present a simplified theoretical model which accurately represents the primary physical mechanisms of the combined convection problem for both assisting and opposing flows in terms of the relevant dimensionless parameters.

A variety of numerical solutions of the governing equations, utilizing solution methods such as local similarity [9, 14], local nonsimilarity, perturbation series [7, 12, 13], and finite difference techniques [6, 11, 19], among others, have been carried out which provide valuable insight into combined forced and natural convective heat transfer. Merkin [10] pointed out the errors associated with a perturbation series numerical solution. Ramachandran *et al.* [17] pointed out that numerical results using local similarity, local nonsimilarity and finite-difference schemes provide identical results for small buoyancy effects, but deviations occur as the buoyancy effects increase.

Although numerical solutions are very helpful in predicting the influence of the various governing parameters behind the investigated phenomenon, a closed-form solution, even if approximate, generally yields more physical insight into the problem, because the functional relationship of the relevant physical parameters is directly observable. Also, a closed-form solution is usually easier to use; for example, a parametric study can be done on a spread sheet, and does not require complex numerical computations.

Acrivos [4] used singular perturbation expansion techniques to approximate the thermal behavior of combined convection with the now common coupling rule [2, 20], which is an addition of solutions (or empirical correlations) of pure forced and pure natural convection, each solution raised to the same power; that is,

$$Nu^n = Nu_F^n \pm Nu_N^n. \quad (1)$$

The form of equation (1) is the basis for empirically

† Author to whom correspondence should be addressed.

NOMENCLATURE

c_p	specific heat at constant pressure [kJ kg^{-1} °C^{-1}]
d	disk diameter [m]
D	test section diameter [m]
g	gravitational acceleration constant [m s^{-2}]
Gr_x	Grashof number, $\rho^2 g\beta(T_w - T_f)x^3/\mu^2$
h	local convective heat transfer coefficient [W m^{-2} °C^{-1}]
$\bar{h}$	average convective heat transfer coefficient [W m^{-2} °C^{-1}]
k	thermal conductivity [W m^{-1} °C^{-1}]
L	total plate length [m]
Nu_x	Nusselt number, hx/k
Pr	Prandtl number, $\mu c_p/k$
Re_x	Reynolds number, $\rho u_f x/\mu$
Ri_x	Richardson number, Gr_x/Re_x^2
t	heat transfer model thickness [m]
T	local temperature [K]
u	local axial velocity [m s^{-1}]
u_f	free-stream velocity [m s^{-1}]
v	local normal velocity [m s^{-1}]
x	axial orientation coordinate [m]
y	normal orientation coordinate [m].

Greek symbols

β	coefficient of thermal expansion [1/K]
$\delta_T(x)$	thickness of thermal boundary layer [m]
$\delta_v(x)$	thickness of hydrodynamic boundary layer [m]
$\varepsilon(x)$	upper limit in energy equation, equation (2)
η	dimensionless velocity coordinate, equation (4)
λ	ratio of boundary layer thicknesses, equation (10)
μ	dynamic fluid viscosity [kg m^{-1} s^{-1}]
ρ	fluid density [kg m^{-3}]
ξ	dimensionless temperature coordinate, equation (5)

Subscripts

f	free-stream value
x	local based on axial distance
w	value at the base of the plate; $y = 0$.

determined exponents, n, for a variety of geometric configurations [1, 2, 20, 21].

Other methods of modeling combined forced and natural convection include replacing the buoyancy force by a pseudo-velocity [22, 23] in the governing equations. Also, by utilizing a modified Reynolds number [24], which incorporates a characteristic buoyancy-induced velocity along with the free stream velocity, Börner [25], and recently Kobus and Wedekind [26], developed empirical correlations for combined forced and natural convective heat transfer. The latter paper developed empirical correlations for different diameter disks and over the entire combined forced and natural convection domain, including the pure forced and pure natural convection limits.

Integral techniques have been successfully applied to numerous engineering problems, including both pure forced and pure natural convective heat transfer [21]. However, only limited attempts have been made to solve the problem of combined forced and natural convection utilizing the integral technique. Acrivos [3] obtained an integral formulation, but ended up using numerical integration to complete the solution, only later to find the results to be in error [4]. Kliegel [15] used an integral model for both assisting and opposing flow assuming fourth-order polynomial distributions for both velocity and temperature profiles, but also ended up solving the simultaneous set of ordinary differential equations describing the thermal and hydrodynamic boundary layer development numerically. Oosthuizen [27] used a similar integral model to obtain a closed-form solution, but only for assisting flow, where the thicknesses of the thermal and hydrodynamic boundary layers were assumed to be equal.

In addition to limited closed-form solutions, only limited experimental data appears to exist in the literature for assisting flow, and even less for opposing flow. The experimental data available for assisting flow, such as that presented by Kliegel [15], Gryzagoridis [16], Hishida *et al.* [8] and Ramachandran *et al.* [17], is for *local* heat transfer; the data obtained by measuring, usually with an interferometer, local heat fluxes. Both Kliegel [15] and Ramachandran *et al.* [17] present limited data for opposing flow where forced convection is initially dominant. However, there is some question as to the validity of part of Kliegel's opposing flow data [17], since it does not approach the forced convection asymptote. To the best knowledge of the authors, no experimental data is available in the literature for local opposing flow heat transfer where natural convection is initially dominant. In addition to the local experimental heat transfer data, Oosthuizen and Bassey [18] presented experimental data for the *average* heat transfer from a vertical flat plate in air under conditions of both assisting and opposing flow, but for a very limited range of the Richardson number, Ri_L.

Since it appears from the existing literature that no one has thus far been successful in doing so, the intent of this research is to obtain a closed-form integral

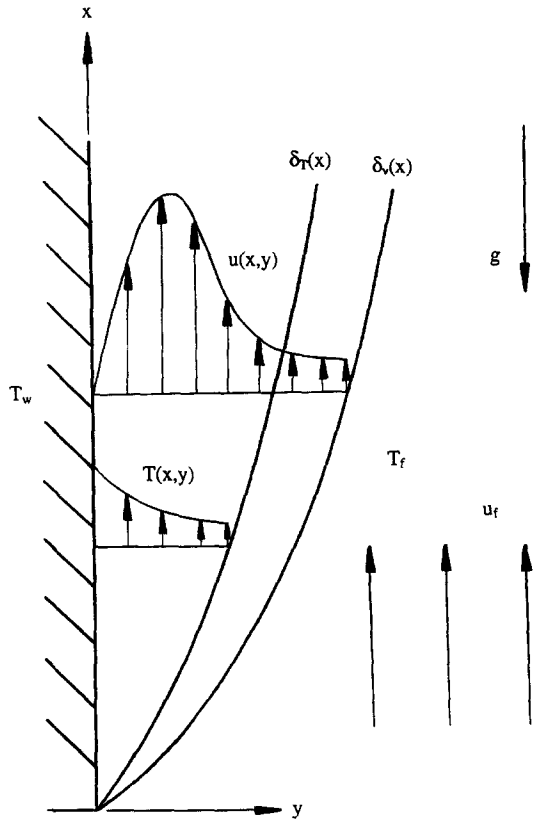

Fig. 1. Schematic of flow geometry and flat plate orientation.

model solution for combined forced and natural convection, for both assisting and opposing flows, and for a Prandtl number other than unity. Also, the intent is to extend the range of experimentally measured *average* heat transfer data for both assisting and opposing flows out to both the pure forced and the pure natural convection asymptotes.

FORMULATION OF THEORETICAL MODEL

Applying the conservation of energy and momentum principles to a finite control volume, extending from the wall to the furthest boundary layer from a vertical flat plate (either thermal or hydrodynamic), as illustrated in Fig. 1, assuming negligible conduction in the x-direction, and utilizing the conservation of mass principle applied to the same control volume, then dividing the resulting equations by the length of the control volume, Δx, and taking the limit as Δx approaches zero, leads to the following governing equations:

Energy equation

$$\frac{\mathrm{d}}{\mathrm{d}x}\int_{y=0}^{\varepsilon(x)} u(T-T_f)\,\mathrm{d}y = -\left(\frac{k}{\rho c_p}\right)\left.\frac{\partial T}{\partial y}\right|_{y=0}. \quad (2)$$

Momentum equation

$$\frac{\mathrm{d}}{\mathrm{d}x}\int_{y=0}^{\delta_v(x)} u(u-u_f)\,\mathrm{d}y = -\left(\frac{\mu}{\rho}\right)\left.\frac{\partial u}{\partial y}\right|_{y=0} + \int_{y=0}^{\delta_T(x)} g\beta(T-T_f)\,\mathrm{d}y. \quad (3)$$

The upper limit of the integral in the energy equation, $\varepsilon(x)$, depends on the particular boundary layer, thermal or hydrodynamic, which extends the greatest distance away from the plate.

Assisting flow

Utilizing the integral technique, a fourth-order polynomial expression is assumed for both the velocity and temperature distributions. Boundary conditions for velocity include no slip at the wall, and free-stream velocity and zero slope at the extent of the hydrodynamic boundary layer. Two more boundary conditions are obtained from the x-component of the Navier–Stokes equation, one where every term is evaluated at the wall, and the other at the extent of the hydrodynamic boundary layer. Boundary conditions for temperature include the wall temperature at the base of the plate and the fluid temperature and zero slope at the extent of the thermal boundary layer. As with the velocity profile, two additional boundary conditions may be obtained by evaluating each term of the differential form of the general energy equation both at the wall and at the extent of the thermal boundary layer. Therefore, utilizing the boundary conditions, the velocity and temperature distributions may be expressed, respectively, after considerable algebraic rearrangement, as

$$u(x,y) = \left[\frac{1}{6}\frac{\rho g\beta(T_w-T_f)}{\mu}\delta_v^2(x)\right](\eta-3\eta^2+3\eta^3-\eta^4) + u_f(2\eta-2\eta^3+\eta^4);\quad \eta = y/\delta_v(x) \quad (4)$$

$$T(x,y) = T_f+(T_w-T_f)(1-2\xi+2\xi^3-\xi^4);\quad \xi = y/\delta_T(x). \quad (5)$$

It should be noted that the velocity distribution for combined forced and natural convection is actually the sum of the velocity profiles for pure natural and pure forced convection [3, 28], as can be seen in equation (4). Substituting equations (4) and (5) into equations (3) and (4), the governing differential equations are expressed, again after considerable algebraic rearrangement and integration, as

$$\frac{\mathrm{d}}{\mathrm{d}x}\left\{\frac{1}{9072\lambda^5}\left[\frac{\rho g\beta(T_w-T_f)}{\mu}\right]^2\delta_T^5(x) + \frac{1}{945\lambda^3}u_f\frac{\rho g\beta(T_w-T_f)}{\mu}\delta_T^3(x) - \frac{37}{315\lambda}u_f^2\delta_T(x)\right\} = \left(\frac{3}{10}-\frac{1}{6\lambda}\right)g\beta(T_w-T_f)\delta_T(x) - 2\left(\frac{\mu}{\rho}\right)\frac{u_f}{\delta_T(x)} \quad (6)$$

$$\frac{\mathrm{d}}{\mathrm{d}x}\left\{\lambda_a(x)\frac{\rho g\beta(T_w-T_f)}{\mu}\delta_T^3(x)+\lambda_b(x)u_f\delta_T(x)\right\}=\left(\frac{k}{\rho c_p}\right)\frac{2}{\delta_T(x)} \quad (7)$$

where

For $\delta_v(x) > \delta_T(x)$,

$$\lambda_a(x)=\frac{1}{6\lambda^2}\left(\frac{\lambda}{15}-\frac{\lambda^2}{14}+\frac{9\lambda^3}{280}-\frac{\lambda^4}{180}\right) \quad (8a)$$

$$\lambda_b(x)=\left(\frac{2\lambda}{15}-\frac{3\lambda^3}{140}+\frac{\lambda^4}{180}\right). \quad (8b)$$

For $\delta_T(x) > \delta_v(x)$,

$$\lambda_a(x)=\frac{1}{6\lambda^2}\left(\frac{1}{20\lambda}-\frac{1}{30\lambda^2}+\frac{1}{140\lambda^3}-\frac{1}{504\lambda^4}\right) \quad (9a)$$

$$\lambda_b(x)=\left(\frac{3}{10}-\frac{3}{10\lambda}+\frac{2}{15\lambda^2}-\frac{3}{140\lambda^3}+\frac{1}{180\lambda^4}\right) \quad (9b)$$

and

$$\lambda=\lambda(x)\equiv\frac{\delta_T(x)}{\delta_v(x)}. \quad (10)$$

If λ is allowed to be unity, the coefficients described by equations (8) and (9) will yield the same values as those presented by Acrivos [3], Kliegel [15] and Oosthuizen [27], $\lambda_a(x)=\lambda_a=11/3024$ and $\lambda_b(x)=\lambda_b=37/315$. This special case generally corresponds to forced and natural convection for fluids with Prandtl numbers near unity.

The coupled momentum and energy equations, (6) and (7), respectively, can not, in general, be solved together except for the special case of Prandtl number equal to unity, that is, where $\lambda=1$. For all other cases, the possible solution is complicated by the fact that the variable, λ, potentially varies along the length of the plate because the buoyancy force increases along the length of the plate, while the inertial force due to the free-stream velocity remains constant [14]. Therefore, for assisting flow, forced convection may dominate near the leading edge of the plate, where λ would be approximately $Pr^{-1/3}$, while natural convection may dominate farther downstream, where λ may approach a different value, depending of course on the pertinent parameters governing the phenomenon. However, assuming that the ratio, λ, of the two distinct boundary layers is approximately constant and equal to the mean value of the boundary layer thickness ratio, $\bar{\lambda}$, the momentum and energy equations become uncoupled and a one-parameter solution† may be obtained by solving the energy equation alone. In this way, λ_a and λ_b are constants and the energy equation, (7), becomes

$$\left\{3\lambda_a\frac{\rho^2 g\beta(T_w-T_f)}{\mu^2}\delta_T^3(x)+\lambda_b\left(\frac{\rho u_f}{\mu}\right)\delta_T(x)\right\}\times\frac{\mathrm{d}\delta_T(x)}{\mathrm{d}x}=2\left(\frac{k}{\mu c_p}\right). \quad (11)$$

Equation (11) is a non-linear, first-order, constant coefficient, non-homogeneous ordinary differential equation expressing the development of the thermal boundary layer, $\delta_T(x)$, with the axial coordinate, x. Separating the variables, and specifying the boundary condition that the thermal boundary layer thickness at the leading edge of the plate, $x=0$, is zero, yields a quadratic equation and can thus be solved with the solution expressed as

$$\delta_T^2(x)=\frac{-2\lambda_b\left(\frac{\rho u_f}{\mu}\right)+\left\{\left[2\lambda_b\left(\frac{\rho u_f}{\mu}\right)\right]^2+\left(\frac{96\lambda_a}{Pr}\right)\frac{\rho^2 g\beta(T_w-T_f)}{\mu^2}x\right\}^{1/2}}{6\lambda_a\frac{\rho^2 g\beta(T_w-T_f)}{\mu^2}} \quad (12)$$

or, in dimensionless form as

$$\left[\frac{\delta_T(x)}{x}\right]^2=\left(\frac{Re_x}{Gr_x}\right)\left\{-\left(\frac{1}{3}\frac{\lambda_b}{\lambda_a}\right)+\left[\left(\frac{1}{3}\frac{\lambda_b}{\lambda_a}\right)^2+\left(\frac{8}{3\lambda_a}\right)\left(\frac{Ri_x}{Pr}\right)\right]^{1/2}\right\}. \quad (13)$$

The local convective heat transfer coefficient, h, is defined as the local heat flux at the wall divided by the temperature difference between the wall and the free-stream. Utilizing Fourier's macroscopic model for conduction and equation (5), the local dimensionless heat transfer coefficient, or Nusselt number, Nu_x, can be expressed in terms of the thermal boundary layer thickness and the axial coordinate, x. Substitution of equation (13) into this expression yields a model for the local dimensionless heat transfer coefficient in terms of the pertinent dimensionless parameters and variables governing the combined convection phenomenon for assisting flow; thus,

$$\frac{Nu_x}{Re_x^{1/2}}=2Ri_x^{1/2}\left\{-\left(\frac{1}{3}\frac{\lambda_b}{\lambda_a}\right)+\left[\left(\frac{1}{3}\frac{\lambda_b}{\lambda_a}\right)^2+\left(\frac{8}{3\lambda_a}\right)\left(\frac{Ri_x}{Pr}\right)\right]^{1/2}\right\}^{-1/2}. \quad (14)$$

Opposing flow; natural convection initially dominating

Unlike assisting flow, there can not be a single integral model solution for opposing flow describing the

† A one-parameter solution has been presented for pure natural convection in heat transfer texts such as Thomas [28] and, although not displaying the true Prandtl number effects over as wide a range as the two-parameter solution [29], the predictive capability is quite good for a limited range of Prandtl numbers.

local heat transfer characteristics over the entire combined convection domain. This is born from the fact that when natural convection initially dominates, the boundary layer originates at the bottom of the plate, and, as illustrated in Fig. 1, increases with increasing x. However, when forced convection initially dominates, the boundary layer originates at the top of the plate, and increases with decreasing x. Thus, the two opposing flow cases will be handled separately and independently of one another.

Assuming natural convection to be initially dominant, the governing equations, (2) and (3), will not change nor will the temperature distribution be altered in any way. In fact, the only difference is a single boundary condition describing the free-stream velocity at the extent of the hydrodynamic boundary layer. Referring to Fig. 1, the direction of the free stream velocity, u_f, will be reversed. This will have the effect of changing the sign preceding the free-stream term in equation (4), and this effect will in turn propagate throughout the outlined analysis describing the assisting flow, yielding the following dimensionless boundary layer development solution:

$$\left[\frac{\delta_T(x)}{x}\right]^2 = \left(\frac{Re_x}{Gr_x}\right)\left\{\left(\frac{1}{3}\frac{\lambda_b}{\lambda_a}\right)+\left[\left(\frac{1}{3}\frac{\lambda_b}{\lambda_a}\right)^2 + \left(\frac{8}{3\lambda_a}\right)\left(\frac{Ri_x}{Pr}\right)\right]^{1/2}\right\}. \quad (15)$$

As can be seen, the only difference between equations (15) and (14) is a change in the sign on one of the terms. The dimensionless heat transfer characteristics for opposing flow where natural convection initially dominates may be expressed as

$$\frac{Nu_x}{Re_x^{1/2}} = 2Ri_x^{1/2}\left\{\left(\frac{1}{3}\frac{\lambda_b}{\lambda_a}\right)+\left[\left(\frac{1}{3}\frac{\lambda_b}{\lambda_a}\right)^2 + \left(\frac{8}{3\lambda_a}\right)\left(\frac{Ri_x}{Pr}\right)\right]^{1/2}\right\}^{-1/2}. \quad (16)$$

It should be noted that although the opposing flow case where natural convection dominates seems to be a simple variation of the assisting flow case, no attempt, to the best knowledge of the authors, has been made to model the problem from the natural convection asymptote, either with the integral technique or otherwise. In fact, it was generally believed that a solution could *only* be obtained from the forced convection asymptote [27].

Opposing flow; forced convection initially dominating

The opposing flow case where forced convection initially dominates will demand the boundary layer development to originate at the top of the plate (Fig. 1). Thus, the entire coordinate system with respect to the boundary layer development is 'switched' to the other end of the plate. Hence, with respect to the reference frame of the new coordinate system, the direction of gravity in Fig. 1 is reversed. This will have the effect of changing the sign of the gravity term, g, in the momentum equation, (3). Because of this sign change, one of the two boundary conditions extracted from the Navier–Stokes equation will change sign and in turn, the sign in front of the buoyancy portion of the velocity distribution, equation (4), will change. The temperature distribution will not be affected because the energy equation, (2), will not be affected by the change in sign of the gravitational term. Thus, following the same method described in the previous two sections, the solution expressing boundary layer development can be obtained yielding

$$\left[\frac{\delta_T(x)}{x}\right]^2 = \left(\frac{Re_x}{Gr_x}\right)\left\{\left(\frac{1}{3}\frac{\lambda_b}{\lambda_a}\right)-\left[\left(\frac{1}{3}\frac{\lambda_b}{\lambda_a}\right)^2 - \left(\frac{8}{3\lambda_a}\right)\left(\frac{Ri_x}{Pr}\right)\right]^{1/2}\right\}. \quad (17)$$

Unlike the previous two cases, a negative sign exists in front of the radical. Also, since a negative sign appears within the radical itself, the solution will yield values for only part of the domain, whereas in the opposing flow case where natural convection initially dominates, the solution is mathematically valid over the entire domain of the Richardson number. The dimensionless heat transfer characteristics for opposing flow where forced convection initially dominates can be expressed as

$$\frac{Nu_x}{Re_x^{1/2}} = 2Ri_x^{1/2}\left\{\left(\frac{1}{3}\frac{\lambda_b}{\lambda_a}\right)-\left[\left(\frac{1}{3}\frac{\lambda_b}{\lambda_a}\right)^2 - \left(\frac{8}{3\lambda_a}\right)\left(\frac{Ri_x}{Pr}\right)\right]^{1/2}\right\}^{-1/2}. \quad (18)$$

Although the form of the solution is the same in all three flow configurations, the sign changes radically alter the predictions of the models.

COMPARISON OF PRESENT MODEL WITH OTHER EXISTING MODELS AND EXPERIMENTAL DATA

The only experimental local convective heat transfer data available for the combined mode of heat transfer is with air. Since air has a Prandtl number near unity ($Pr = 0.72$), the ratio of the thickness of the thermal and hydrodynamic boundary layers, λ, is about 1.10 for pure natural convection [30], and $\lambda = Pr^{-1/3}$, approximately 1.116, for pure forced convection. Therefore, it seems reasonable to assume that λ does not vary significantly along the length of the plate. Thus, a good estimate of the average boundary layer thickness ratio, $\bar{\lambda}$, would be the *algebraic mean* of the two extreme limits; pure forced and pure natural convection. Incidentally, it can be observed from the research of Ostrach [30, 31] that the boundary layer thickness ratio, λ, for pure natural convection does

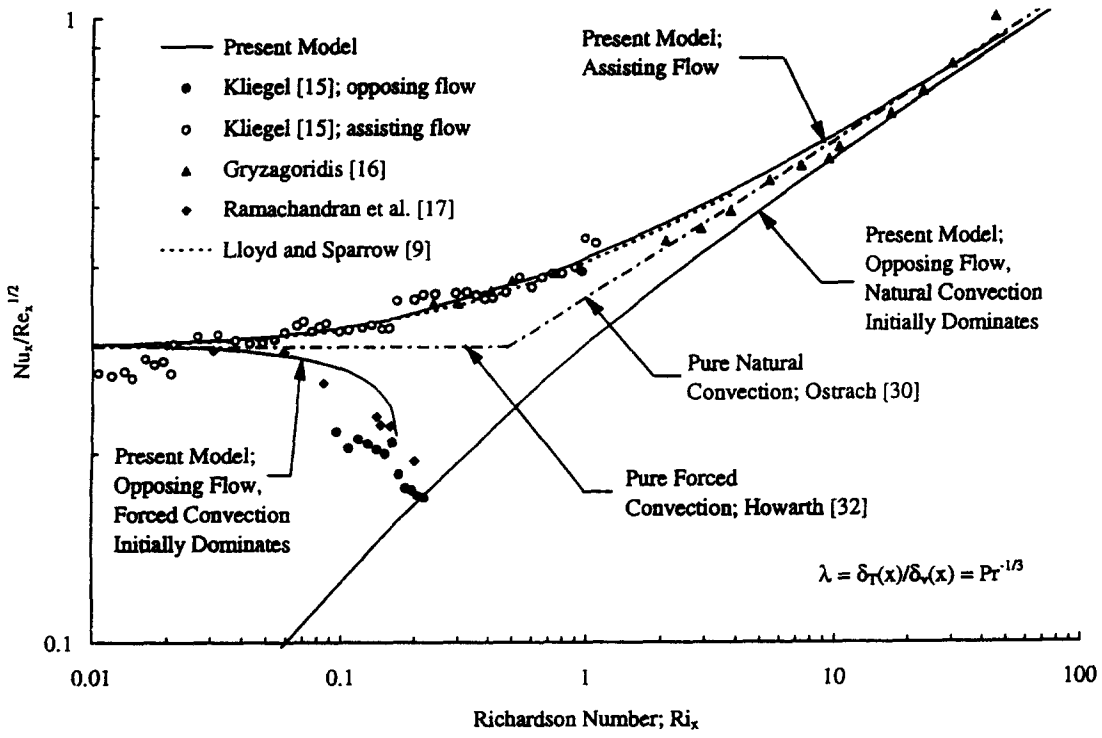

Fig. 2. Local combined forced and natural convective heat transfer characteristics from an isothermal vertical flat plate in air; assisting and opposing flows.

not vary significantly from what is predicted for classic forced convection, that is, $\lambda = Pr^{-1/3}$. In fact, for $0.72 \leqslant Pr \leqslant 10$, the difference in these values is less than 6%†. Hence, $\lambda = \bar{\lambda} = Pr^{-1/3}$ is a very good approximation for this important range of Prandtl numbers and is thus recommended for the present model. Utilizing this approximation, excellent agreement can be seen in Fig. 2 to exist between the present integral model, the available experimental data for assisting flow in air and the numerical solution of Lloyd and Sparrow‡ [9].

In the case of opposing flow, the only available experimental data, to the best knowledge of the authors, seems to be between the forced convection asymptote and the point referred to in the literature as the *separation point* [17], represented in Fig. 2 by the last of the data§ of Kliegel [15] and Ramachandran *et al.* [17], at a Richardson number of approximately 0.2. Note that the combined convection Nusselt number, Nu_x, at the point of separation is significantly lower than that of the pure forced convection asymptote. The present integral model developed for opposing flow where forced convection effects initially dominate, apparently does not reach the point of separation, because the numerical values under the radical of equation (18) become negative for Richardson numbers‖, $Ri_x > 0.18$.

The physics behind the point of separation in combined convection is not all clear because of the lack of experimental data in the neighborhood of the phenomenon. Conceptually, however, this point is where the velocity at the base of the flat plate has zero slope, and therefore only pure *conduction* heat transfer from the plate to the air may occur. It is believed that for Richardson numbers beyond the value where the separation occurs, natural convection effects must become more dominant and thus there must in fact be a flow reversal, until, in the limit as the Richardson

† This range of Prandtl numbers encompasses many engineering fluids, such as the common gases and liquids, e.g. water. For $Pr = 100$ and 1000, the difference between $Pr^{-1/3}$ and the values obtained by Ostrach [30, 31] is 16 and 33%, respectively, while for a Prandtl number of 0.01, corresponding to liquid metals, the difference is significantly higher at 76%.

‡ It should be noted that Lloyd and Sparrow [9] indicated that their numerical solution is restricted to $Ri_x \leqslant 5$ due to the restriction of the similarity technique to small buoyancy effects.

§ The whole of the opposing flow data of Kliegel [15] was not displayed as there was some question of its accuracy, addressed by Ramachandran *et al.* [17], born out of the fact that the data asymptoted about 35% lower than the pure forced convection boundary layer model [32] predicted. However, it is believed that Kliegel's data near the point of separation is accurate since it corresponds very closely with the data of Ramachandran *et al.* [17].

‖ It is interesting to note that the numerical solution presented by Ramachandran *et al.* [17] diverges for a Richardson number, $Ri_x \geqslant 0.18$. Also, as mentioned by Ramachandran *et al.*, Hishida *et al.* [8] predicted the point of separation to occur at a Richardson number of 0.25, but it was not clear as to how this value was determined.

number becomes increasingly large, any experimental data *must* approach the pure natural convection asymptote from below.

It is interesting to note that the integral model for opposing flow, developed on the assumption that natural convection effects initially dominate, seems to intersect the point of separation precisely. Regrettably, no experimental data exists demonstrating the accuracy of this particular opposing flow solution up to the natural convection asymptote, although the conceptual argument is made on the basis of physical reasoning that any experimental data *must* approach this asymptote. Clearly, the area of combined forced and natural convective heat transfer is still in need for experimental data, both for opposing flow, and for fluids of Prandtl numbers other than 0.72, since it appears that the only heat transfer data currently available in the literature is for air.

AVERAGE HEAT TRANSFER

Theoretical model

Although the solution for predicting the local heat transfer characteristics is very useful in gaining valuable physical insight into the governing physical mechanisms, the average heat transfer predictions are generally of greater practical application. The average Nusselt number can be expressed in terms of the average convective heat transfer coefficient, which in turn may be expressed through the mean value theorem in terms of the local heat transfer coefficient. Substituting equations (13), (15) and (17), into this expression and integrating, the solutions for the average heat transfer coefficient may be obtained, albeit after considerable algebraic rearrangement and variable transformations. Thus,

Assisting flow.

$$\frac{Nu_L}{Re_L^{1/2}} = \frac{2\lambda_b^{1/2} Pr}{3\sqrt{3}}\left(\frac{\lambda_a}{\lambda_b^2}\right)^{-1/2} Ri_L^{-1/2} \times \left\{\frac{1}{2}\left[1+\frac{24}{Pr}\left(\frac{\lambda_a}{\lambda_b^2}\right)Ri_L\right]^{1/2}+1\right\} \times \left\{\left[1+\frac{24}{Pr}\left(\frac{\lambda_a}{\lambda_b^2}\right)Ri_L\right]^{1/2}-1\right\}^{1/2}. \quad (19)$$

Opposing flow; natural convection initially dominates.

$$\frac{Nu_L}{Re_L^{1/2}} = \frac{2\lambda_b^{1/2} Pr}{3\sqrt{3}}\left(\frac{\lambda_a}{\lambda_b^2}\right)^{-1/2} Ri_L^{-1/2} \times \left\{\left\{\frac{1}{2}\left[1+\frac{24}{Pr}\left(\frac{\lambda_a}{\lambda_b^2}\right)Ri_L\right]^{1/2}-1\right\} \times \left\{1+\left[1+\frac{24}{Pr}\left(\frac{\lambda_a}{\lambda_b^2}\right)Ri_L\right]^{1/2}\right\}^{1/2}+\frac{\sqrt{2}}{2}\right\}. \quad (20)$$

Opposing flow; forced convection initially dominates.

$$\frac{Nu_L}{Re_L^{1/2}} = \frac{2\lambda_b^{1/2} Pr}{3\sqrt{3}}\left(\frac{\lambda_a}{\lambda_b^2}\right)^{-1/2} Ri_L^{-1/2} \times \left\{\frac{1}{2}\left[1-\frac{24}{Pr}\left(\frac{\lambda_a}{\lambda_b^2}\right)Ri_L\right]^{1/2}+1\right\} \times \left\{1-\left[1-\frac{24}{Pr}\left(\frac{\lambda_a}{\lambda_b^2}\right)Ri_L\right]^{1/2}\right\}^{1/2}. \quad (21)$$

As with the three solutions describing the *local* heat transfer characteristics, virtually all the differences between the three different flow configurations for the average heat transfer characteristics manifest themselves in sign changes, except for the opposing flow case where natural convection initially dominates. This is seen in equation (20), which contains an additional constant which is not present in the other two solutions. Also, the negative terms within the radicals of equation (21) restricts the range of applicability in terms of the Richardson number, which is consistent with the restriction on the local heat transfer solution. It should be noted that, to the best knowledge of the authors, no attempt has previously been made in the literature, either numerical or analytical, to predict the average heat transfer coefficient of a flat plate under the simultaneous influence of buoyancy and inertia, except via the combining rule of equation (1).

Experimental apparatus and measurement techniques

To the best knowledge of the authors, the only experimental data available in the literature for the *average* convective heat transfer coefficient for combined forced and natural convection is presented by Oosthuizen and Bassey [18]. This data is only for a very limited range of the Richardson number. Therefore, one of the objectives of the current research is to supplement the available experimental data in the literature.

The rectangular plates that were used as experimental heat transfer models for the present experimental data were modified from circular disk-type *thermistors*, which were used successfully in prior experimental work involving flow past stationary circular disks [26, 33] for pure forced, pure natural and combined forced and natural convective heat transfer. The test models were made by carefully grinding the edges of a circular disk into a rectangular shape. Thermistors were chosen as the heat transfer models because they provided a unique combination for indirectly measuring the surface temperature and the convective heat transfer rate. The thermistor was self-heated by means of Joule heating. Conduction losses through the thermistor lead wires (0.127 mm dia) were minimized by using constantan wire [26].

Using an electrical circuit such as the one suggested by Wedekind [33] and later used by Kobus and Wede-

kind [26], the thermistor current and resistance can be accurately and simultaneously measured during self-heating. This makes it possible to indirectly measure not only the convective heat transfer rate, but the average temperature of the thermistor as well; the latter by having pre-calibrated the resistance/temperature characteristics of each thermistor heat transfer model. Thermistors have a high resistance coefficient, therefore, the heat transfer surface temperature could be indirectly measured quite accurately without the many difficulties encountered in attempting to measure the surface temperature by conventional means.

The experimental apparatus and the particular technique involved in obtaining indirect measurements of the convective heat transfer rate and surface temperature will only be summarized here, as it is discussed in detail in earlier papers [26, 33]. Essentially, the average convective heat transfer coefficient can be expressed in terms of the heat transfer rate, the heat transfer surface area, and the temperature difference between the surface and the fluid. The thermistor temperature may be maintained during a test by adjusting the power supply voltage such that the thermistor–standard resistor voltage ratio remains constant.

It is interesting to note that the experimental work of Oosthuizen and Bassey [18] utilized similar techniques to indirectly measure the temperature of platinum strips that were the experimental heat transfer models by measuring the voltage drop across the strips and utilizing the tabulated value of the resistance–temperature coefficient of platinum. However, it should be pointed out that the resistance–temperature coefficient of thermistor material is much larger than that of platinum, such that a small temperature difference causes a sizable resistance change, hence significantly reducing possible experimental error in measuring the resistance and in turn indirectly the surface temperature.

A schematic of the experimental apparatus, which amounts to a miniature wind tunnel made possible by the small size of the thermistor heat transfer models, is shown in Fig. 3 in the assisting flow configuration. For the opposing flow experimentation, the diffuser section was directly connected to a variable-speed blower assembly which would draw air out through the bottom of the test section, effectively providing flow in the same direction as gravity, thus opposing the buoyancy force. Also, for the opposing flow configuration, a velocity development length was placed upstream of the test section. The free-stream air temperature was measured with a thermocouple probe upstream of the heat transfer model. A variable d.c. power supply was used as the power source to self-heat the thermistor. Digital multimeters were used to simultaneously measure the voltage drop across the thermistor and standard resistor of known value, which was connected in series with the thermistor [26, 33].

Uniformity of velocity upstream of the heat transfer model was measured either by a pitot-tube or a hot wire anemometer traverse and varied with the flow-rate, because, for very low Reynolds numbers, based on the inside diameter of the test section, Re_D, the

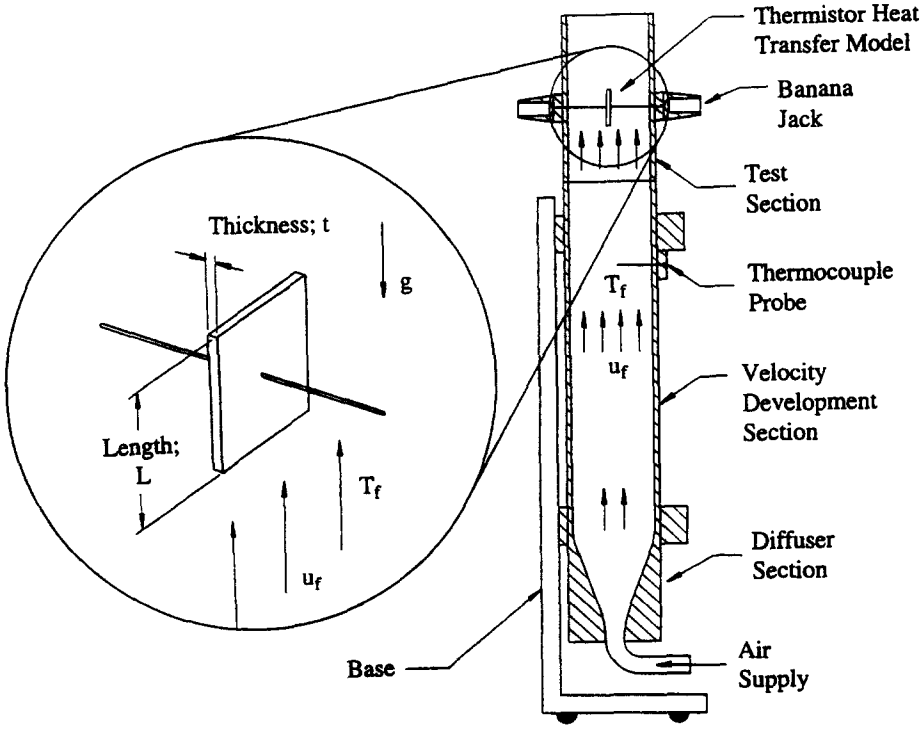

Fig. 3. Schematic of experimental apparatus and flat plate orientation.

flow in the velocity development section was clearly laminar, while for the higher flowrates it was turbulent and nearly uniform [33]. Because of the low flowrates encountered in combined forced and natural convection experimentation, a pitot tube could not be used over the lower range of available flowrates. Therefore, variable-area flowmeters, the smallest of which had a full-scale reading of 7.87 cubic centimeters per second, were used upstream of the diffuser section to measure the volumetric flowrate and thus indirectly the average velocity. However, because of the very low Reynolds numbers, Re_D, encountered in the velocity development section (well below 2000 for the lower flowrates), the average velocity could potentially vary significantly from the true centerline velocity flowing past the heat transfer models. Therefore, calibration experiments were performed to establish a relationship between the average velocity measured with the variable-area flowmeters and the centerline velocity measured with a hot-wire anemometer, in

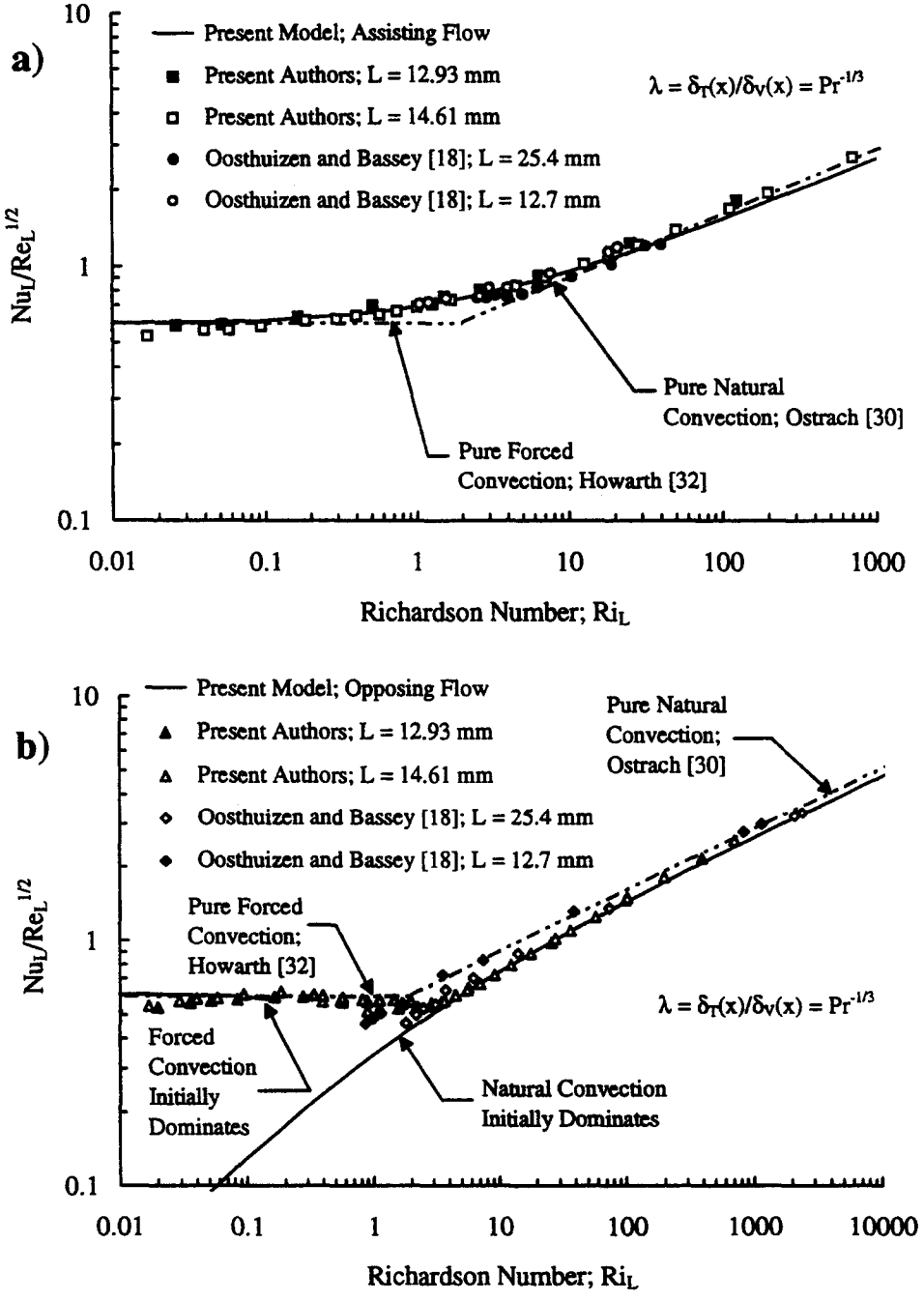

Fig. 4. Average combined forced and natural convective heat transfer characteristics from an isothermal vertical flat plate in air; (a) assisting flow, (b) opposing flow.

both assisting and opposing flow configurations. The air velocity was varied by controlling the inlet air flowrate for assisting flow, or blower speed for opposing flow. Experimental uncertainties were identical to those mentioned by Kobus and Wedekind [26] and will not be repeated here.

Two different experimental flat plate heat transfer models were tested, the lengths ranging from 12.93 to 14.61 mm, and a thickness to length aspect ratio, (t/L), from 0.096 to 0.108. The edges of the flat plates were relatively sharp (edge radius $\cong$ 0.04 mm). For the full range of measurements taken, combined forced and natural convection free-stream air velocities, v_f, ranged from 0.006 to 3 m s^{-1} (0.02–10 ft s^{-1}), temperature differences $(T-T_f)$ were held constant at approximately 56°C (100°F), and the convective heat transfer coefficients, h, ranged from 11.4–40 W $m^{-2}°C^{-1}$ (2–7 Btu $hr^{-1}-ft^{-2}°F^{-1}$). Property values for air, which was at atmospheric pressure, were evaluated at the film temperature, T_{film}, where $T_{film}=(T_w+T_f)/2$. Reynolds numbers, Re_L, ranged from 3 to 2000.

Experimental data; assisting flow

A comparison of the present model and the experimental data from the present research for assisting combined forced and natural convective heat transfer is depicted in dimensionless form in Fig. 4(a), along with the experimental data of Oosthuizen and Bassey [18]. Excellent agreement is clearly seen to exist. The present experimental data extends the currently available experimental data in the literature by several orders of magnitude, and demonstrates excellent agreement with both the natural and forced convection asymptotes for large and small values of the Richardson number, respectively. Also, excellent agreement is seen with the experimental data available in the literature [18].

Experimental data; opposing flow

The two solutions of the present theoretical model are compared with the experimental results of the present research for opposing flow heat transfer, and are depicted in dimensionless form in Fig. 4(b), along with the experimental data of Oosthuizen and Bassey [18]. Again, excellent agreement can be observed between the two solutions of the present model, corresponding to the cases where forced and natural convection initially dominate, the present experimental data and that of Oosthuizen and Bassey [18]. As can be seen from the graph, there is a range of the Richardson number between the point where the opposing flow solution based on initially dominant forced convection is no longer valid ($Ri_L \cong 0.2$) and where the solution based on initially dominant natural convection diverges from the experimental data ($Ri_L \cong 1$). Also, the solution which assumes forced convection to be initially dominant does not seem to extend very far into the combined convection regime. This is seen to be a *mathematical* limitation of the present model. Also, the experimental data presented by Oosthuizen and Bassey [18], corresponding to a length, L, of 12.7 mm, seems to be slightly high for the entire experimental domain of Richardson numbers presented, and may be due to experimental uncertainty in measuring the average temperature of their experimental heat transfer models as was discussed earlier.

CONCLUSIONS

The closed-form solutions to the theoretical model presented in the current research should predict well for fluids with Prandtl numbers other than $Pr = 0.72$, although there is limited basis for comparison at this time, as there is neither sufficient experimental data nor numerical solutions in the current literature. To the best knowledge of the authors, experimental heat transfer data for combined forced and natural convection is only available for air at this time. However, certain simplifying assumptions in formulating the present model indicate that the range of Prandtl numbers for which the solutions may be applicable are for $0.72 \leqslant Pr \leqslant 10$. Incidentally, the authors have made an initial attempt to carry out experiments parallel to those presented in this paper, but with *water* rather than air. However, several experimental difficulties have limited the experimentation at this time. It is hoped that once the experimental difficulties are resolved, the model may be shown to predict heat transfer coefficients for water as well. This will be the subject of future research.

Acknowledgments—The authors would like to acknowledge the work of Stu Dorsey and Frank Cox, from the Oakland University Instrument Shop, who constructed the experimental test sections. Also, thanks go to Len Brown, manager of the electronics shop, whose assistance and suggestions with the circuitry in the experimental apparatus were very helpful to the current research.

REFERENCES

1. S. W. Churchill, A comprehensive correlating equation for laminar, assisting, forced and free convection, *AIChE J.* **23**, 10–16 (1977).
2. B. Gebhart, Y. Jaluria, R. L. Mahajan and B. Sammakia, *Buoyancy-Induced Flows and Transport*. Hemisphere, New York (1988).
3. A. Acrivos, Combined laminar free- and forced-convection heat transfer in external flows, *AIChE J.* **4**, 285–289 (1958).
4. A. Acrivos, On the combined effect of forced and free convection heat transfer in laminar boundary layer flows, *Chem. Engng Sci.* **21**, 343–352 (1966).
5. G. Wilks, Heat transfer coefficients for combined forced and free convection flow about a semi-infinite, isothermal plate, *Int. J. Heat Mass Transfer* **19**, 951–953 (1976).
6. S. Tsuruno and I. Iguchi, Mechanism of heat and momentum transfer of combined free and forced convection with opposing flow, *J. Heat Transfer* **101**, 573–575 (1979).
7. S. Esghy, Forced-flow effects on free-convection flow and heat transfer, *J. Heat Transfer* **86**, 290–291 (1964).
8. K. Hishida, A. Yoshida and M. Maeda, Buoyancy effects

on boundary layer flow and forced convective heat transfer over a vertical isothermally heated flat plate, *ASME-JSME Thermal Engineering Joint Conference Proceedings*, Honolulu, Hawaii, Vol. 3, pp. 163–168 (1983).
9. J. R. Lloyd and E. M. Sparrow, Combined forced and free convection flow on vertical surfaces, *Int. J. Heat Mass Transfer* **13,** 434–438 (1970).
10. J. H. Merkin, The effect of buoyancy forces on the boundary-layer flow over a semi-infinite vertical flat plate in a uniform free stream, *J. Fluid Mech.* **35,** 439–450 (1969).
11. P. H. Oosthuizen and R. Hart, A numerical study of laminar combined convective flow over flat plates, *J. Heat Transfer* **95,** 60–63 (1973).
12. E. M. Sparrow and J. L. Gregg, Buoyancy effects in forced-convection flow and heat transfer, *J. Heat Transfer* **81,** 133–134 (1959).
13. A. A. Szewczyk, Combined forced and free-convection laminar flow, *J. Heat Transfer* **86,** 501–507 (1964).
14. L. S. Yao, Two-dimensional mixed convection along a flat plate, *J. Heat Transfer* **109,** 440–445 (1989).
15. J. R. Kliegel, Laminar free and forced convection heat transfer from a vertical flat plate, Ph.D. Thesis, University of California, Berkeley (1959).
16. J. Gryzagoridis, Combined free and forced convection from an isothermal vertical plate, *Int. J. Heat Mass Transfer* **18,** 911–916 (1975).
17. N. Ramachandran, B. F. Armaly and T. S. Chen, Measurements and predictions of laminar mixed convection flow adjacent to a vertical surface, *J. Heat Transfer* **107,** 636–641 (1985).
18. P. H. Oosthuizen and M. Bassey, An experimental study of combined forced- and free-convection heat transfer from flat plates to air at low Reynolds numbers, *J. Heat Transfer* **95,** 120–121 (1973).
19. M. S. Raju, X. Q. Liu and C. K. Law, A formulation of combined forced and free convection past horizontal and vertical surfaces, *Int. J. Heat Mass Transfer* **27,** 2215–2224 (1984).
20. F. P. Incropera and D. P. DeWitt, *Fundamentals of Heat and Mass Transfer* (3rd Edn), Chap. 6, 7 and 9. Wiley, New York (1990).
21. S. Kakac and Y. Yener, *Convective Heat Transfer* (2nd Edn), Chap. 5. CRC Press, Ann Arbor, MI (1995).
22. E. Ruckenstein and A. Rajagopalan, Simple algebraic method for obtaining the heat or mass transfer coefficients under mixed convection, *Chem. Engng Commun.* **4,** 15–39 (1980).
23. M. R. Cameron, D. R. Jeng and K. J. DeWitt, Mixed forced and natural convection from two-dimensional or axisymmetric bodies of arbitrary contour, *Int. J. Heat Mass Transfer* **34,** 582–587 (1991).
24. O. Krischer and G. Loos, Wärme- und Stoffaustausch bei erzwungener Strömung an Körpern verschiedener Form, Teil 1, *Chem. Ing. Tech.* **30,** 31 (1958).
25. H. Börner, Über den Wärme- und Stoffübertragang um umspülten Einzelkorpern bei überlagerung von freier und erzwyngener Strömung, *Ver. Deut. Ing. Forschungsheft*, no. 512 (1965).
26. C. J. Kobus and G. L. Wedekind, An experimental investigation into forced, natural and combined forced and natural convective heat transfer from stationary isothermal circular disks, *Int. J. Heat Mass Transfer* **38,** 3329–3339 (1995).
27. P. H. Oosthuizen, A note on the combined free and forced convective laminar flow over a vertical isothermal plate, *South African Mech. Engnr* **15,** 8–13 (1965).
28. L. C. Thomas, *Heat Transfer*, Chap. 8–9. Prentice-Hall, Englewood Cliffs, NJ (1992).
29. J. P. Holman, *Heat Transfer* (7th Edn), Chap. 5–7. McGraw-Hill, New York (1990).
30. S. Ostrach, An analysis of laminar free-convection and heat transfer about a flat plate parallel to the direction of the generating body force, NACA Report 1111 (1953).
31. S. Ostrach, An analysis of laminar free-convection and heat transfer about a flat plate parallel to the direction of the generating body force, NACA Report 2635 (1952).
32. L. Howarth, On the solution of the laminar boundary layer equations, *Proc. R. Soc. Lond.* **164A,** 547–579 (1938).
33. G. L. Wedekind, Convective heat transfer measurement involving flow past stationary circular disks, *J. Heat Transfer* **111,** 1098–1100 (1989).